JCI The Journal of Clinical Investigation

c-Met–mediated endothelial plasticity drives aberrant vascularization and chemoresistance in glioblastoma

Menggui Huang, … , Constantinos Koumenis, Yi Fan

J Clin Invest. 2016;126(5):1801-1814. https://doi.org/10.1172/JCI84876.

Research Article **Oncology**

Aberrant vascularization is a hallmark of cancer progression and treatment resistance. Here, we have shown that endothelial cell (EC) plasticity drives aberrant vascularization and chemoresistance in glioblastoma multiforme (GBM). By utilizing human patient specimens, as well as allograft and genetic murine GBM models, we revealed that a robust endothelial plasticity in GBM allows acquisition of fibroblast transformation (also known as endothelial mesenchymal transition [Endo-MT]), which is characterized by EC expression of fibroblast markers, and determined that a prominent population of GBM-associated fibroblast-like cells have EC origin. Tumor ECs acquired the mesenchymal gene signature without the loss of EC functions, leading to enhanced cell proliferation and migration, as well as vessel permeability. Furthermore, we identified a c-Met/ETS-1/matrix metalloproteinase–14 (MMP-14) axis that controls VE-cadherin degradation, Endo-MT, and vascular abnormality. Pharmacological c-Met inhibition induced vessel normalization in patient tumor–derived ECs. Finally, EC-specific KO of *Met* inhibited vascular transformation, normalized blood vessels, and reduced intratumoral hypoxia, culminating in suppressed tumor growth and prolonged survival in GBM-bearing mice after temozolomide treatment. Together, these findings illustrate a mechanism that controls aberrant tumor vascularization and suggest that targeting Endo-MT may offer selective and efficient strategies for antivascular and vessel normalization therapies in GBM, and possibly other malignant tumors.

c-Met–mediated endothelial plasticity drives aberrant vascularization and chemoresistance in glioblastoma

Menggui Huang,[1] Tianrun Liu,[1,2] Peihong Ma,[1] R. Alan Mitteer Jr.,[1] Zhenting Zhang,[1] Hyun Jun Kim,[1] Eujin Yeo,[1] Duo Zhang,[1] Peiqiang Cai,[1] Chunsheng Li,[3] Lin Zhang,[3] Botao Zhao,[4] Laura Roccograndi,[5] Donald M. O'Rourke,[5] Nadia Dahmane,[5] Yanqing Gong,[6] Constantinos Koumenis,[1] and Yi Fan[1,5]

[1]Department of Radiation Oncology, University of Pennsylvania Perelman School of Medicine, Philadelphia, Pennsylvania, USA. [2]Division of Head and Neck Surgery, Department of Otorhinolaryngology, The Sixth Affiliated Hospital of Sun Yat-sen University, Guangzhou, China. [3]Department of Obstetrics and Gynecology, University of Pennsylvania Perelman School of Medicine, Philadelphia, Pennsylvania, USA. [4]School of Life Sciences, Shanghai University, Shanghai, China. [5]Department of Neurosurgery and [6]Division of Human Genetics and Translational Medicine, Department of Medicine, University of Pennsylvania Perelman School of Medicine, Philadelphia, Pennsylvania, USA.

Aberrant vascularization is a hallmark of cancer progression and treatment resistance. Here, we have shown that endothelial cell (EC) plasticity drives aberrant vascularization and chemoresistance in glioblastoma multiforme (GBM). By utilizing human patient specimens, as well as allograft and genetic murine GBM models, we revealed that a robust endothelial plasticity in GBM allows acquisition of fibroblast transformation (also known as endothelial mesenchymal transition [Endo-MT]), which is characterized by EC expression of fibroblast markers, and determined that a prominent population of GBM-associated fibroblast-like cells have EC origin. Tumor ECs acquired the mesenchymal gene signature without the loss of EC functions, leading to enhanced cell proliferation and migration, as well as vessel permeability. Furthermore, we identified a c-Met/ETS-1/matrix metalloproteinase–14 (MMP-14) axis that controls VE-cadherin degradation, Endo-MT, and vascular abnormality. Pharmacological c-Met inhibition induced vessel normalization in patient tumor–derived ECs. Finally, EC-specific KO of *Met* inhibited vascular transformation, normalized blood vessels, and reduced intratumoral hypoxia, culminating in suppressed tumor growth and prolonged survival in GBM-bearing mice after temozolomide treatment. Together, these findings illustrate a mechanism that controls aberrant tumor vascularization and suggest that targeting Endo-MT may offer selective and efficient strategies for antivascular and vessel normalization therapies in GBM, and possibly other malignant tumors.

Introduction

Overgrown, abnormal vasculature characterizes the microenvironment that fuels cancer progression and induces therapeutic resistance in malignant solid tumors (1–3). Glioblastoma multiforme (GBM), the grade IV glioma, is among the most lethal of human malignancies, distinguished by prominent vascularity and extraordinary vascular abnormality of unknown etiology. GBM is the most common and most aggressive primary brain tumor in humans, with a current median survival of about 14 months (4). Most GBM tumors are refractory to conventional cytotoxic therapies (5). Antiangiogenesis therapies, primarily targeting angiogenic factors including VEGF-A and their receptors, have been developed and exploited in recent years; however, the therapeutic benefits have been small and transient (6, 7), due to compensatory activation of other angiogenic factors, acquired treatment resistance, and other unidentified mechanisms.

Cell plasticity in vascular endothelial cells (ECs) has been well characterized in embryogenesis (8). Likewise, previous work has documented the robust ability of EC to transdifferentiate and transition into hematopoietic cells and stem cells during embryonic development (9–13). In pathological settings including myocardial infarction, renal and liver fibrosis, ossifying myositis, vascular inflammation, and cerebral cavernous malformation, ECs undergo endothelial mesenchymal transition (Endo-MT) to de novo generate fibroblasts, stem-like cells, and smooth muscle cells (14–20). Recent data shows the existence of Endo-MT in melanoma and Kaposi sarcoma (21, 22). However, the role of EC plasticity in cancer progression, particularly in tumor-associated angiogenesis, remains elusive. Here, we identify robust Endo-MT in GBM. Interestingly, tumor-associated ECs acquire fibroblast phenotypes including high motility and invasiveness but retain key endothelial functions without cell fate transition, inducing abnormal vascularization and therapeutic resistance. Thus, Endo-MT represents a previously unidentified cellular mechanism for aberrant vascularization, and targeting Endo-MT may serve as a novel therapeutic strategy for the treatment of GBM and other malignant solid tumors.

Results

Robust Endo-MT in GBM-associated vasculature. We investigated the role of EC plasticity in GBM, initially focusing on a possible mesenchymal transition. $CD31^+$ ECs were isolated from GBM tumors in human patients, and no contamination with other cell types was validated by EC-specific acetylated LDL (Ac-LDL) absorption in

Conflict of interest: The authors have declared that no conflict of interest exists.
Submitted: September 30, 2015; **Accepted:** February 18, 2016.
Reference information: *J Clin Invest*. 2016;126(5):1801–1814. doi:10.1172/JCI84876.

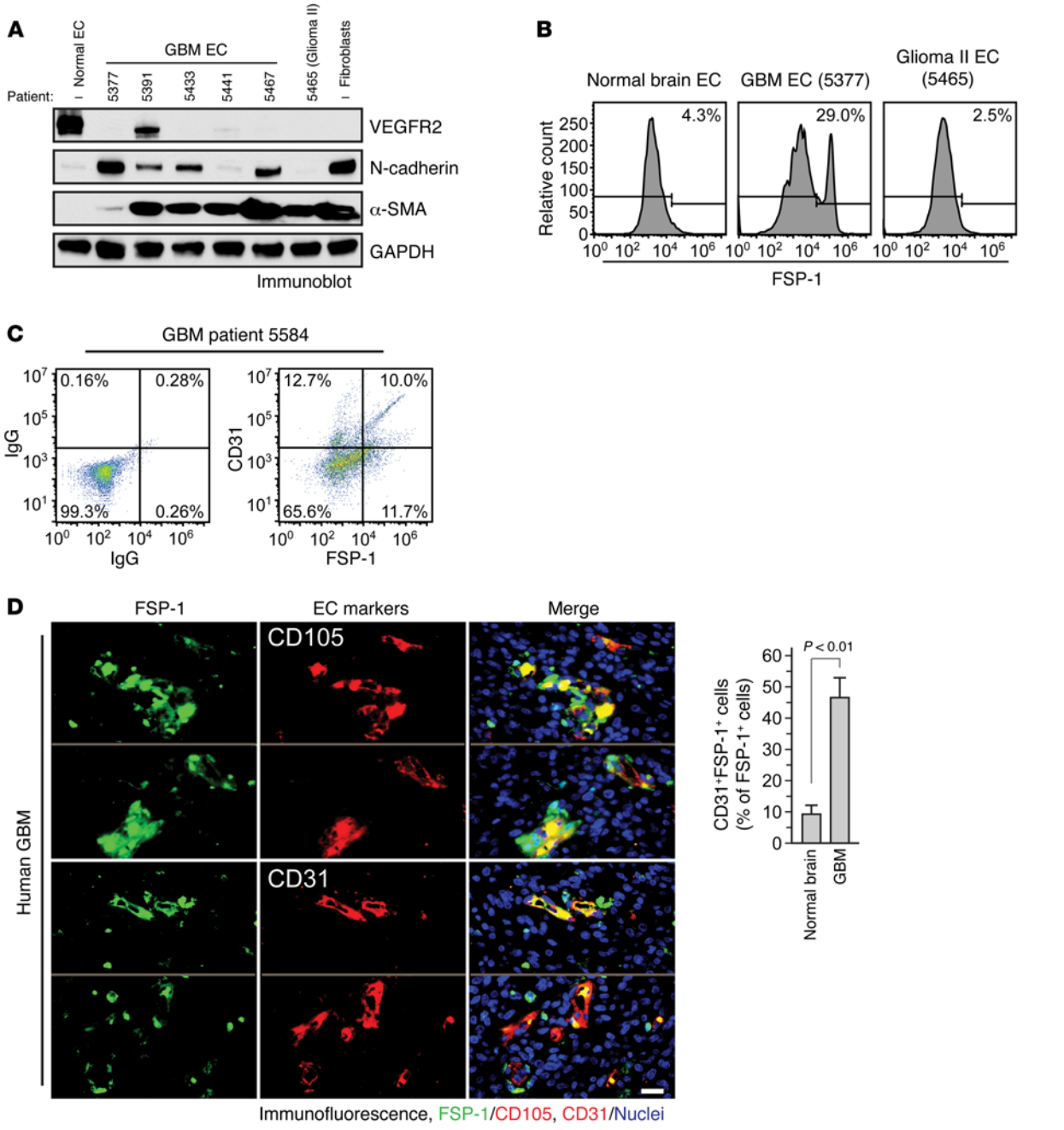

Figure 1. Mesenchymalization in human GBM-associated ECs. Single-cell suspensions were prepared from surgical specimens of GBM patient tumors (n = 15 patients). (**A** and **B**) ECs were isolated from the cell suspensions by CD31 antibody–based magnetic-activating cell sorting. (**A**) Cell lysates were resolved by SDS-PAGE, followed by immunoblot analysis. Representative data are shown from 3 independent experiments. (**B**) Cells were stained with anti–FSP-1 antibody and analyzed by flow cytometry. Representative data are shown from 6 patients. (**C**) Whole-tumor cell suspensions were stained with anti–FSP-1 and -CD31 or control IgGs and analyzed by flow cytometry. Representative data are shown from 3 patients. (**D**) Sections of surgical specimens from normal brain and GBM patients were probed with anti–FSP-1, -CD105, and -CD31 antibodies. Left, representative images. Right, quantitative analysis of colocalization of $CD31^+$ ECs with $FSP\text{-}1^+$ fibroblast–like cells (n = 5 patients, mean ± SEM, unpaired t test). Scale bar: 50 μm.

all cells and lack of expression of pericyte-specific marker NG-2 (not shown). GBM tumor–derived ECs exhibited fibroblast-like elongated morphology when cultured (Supplemental Figure 1; supplemental material available online with this article; doi:10.1172/JCI84876DS1). Immunoblot analysis revealed that these cells expressed multiple mesenchymal genes including N-cadherin (4 in 5 patients), α–smooth muscle actin (α-SMA), and fibroblast-specific protein-1 (FSP-1), while the expression of VEGF receptor-2 (VEGFR2) was diminished in tumor ECs (Figure 1, A and B), suggesting that GBM-associated ECs have mesenchymal characteristics. Likewise, flow cytometry analysis with single-cell suspension from surgical GBM specimens showed that over 40% of $CD31^+$ ECs expressed FSP-1 (Figure 1C). Moreover, immunofluorescence studies of human GBM samples revealed a robust colocalization

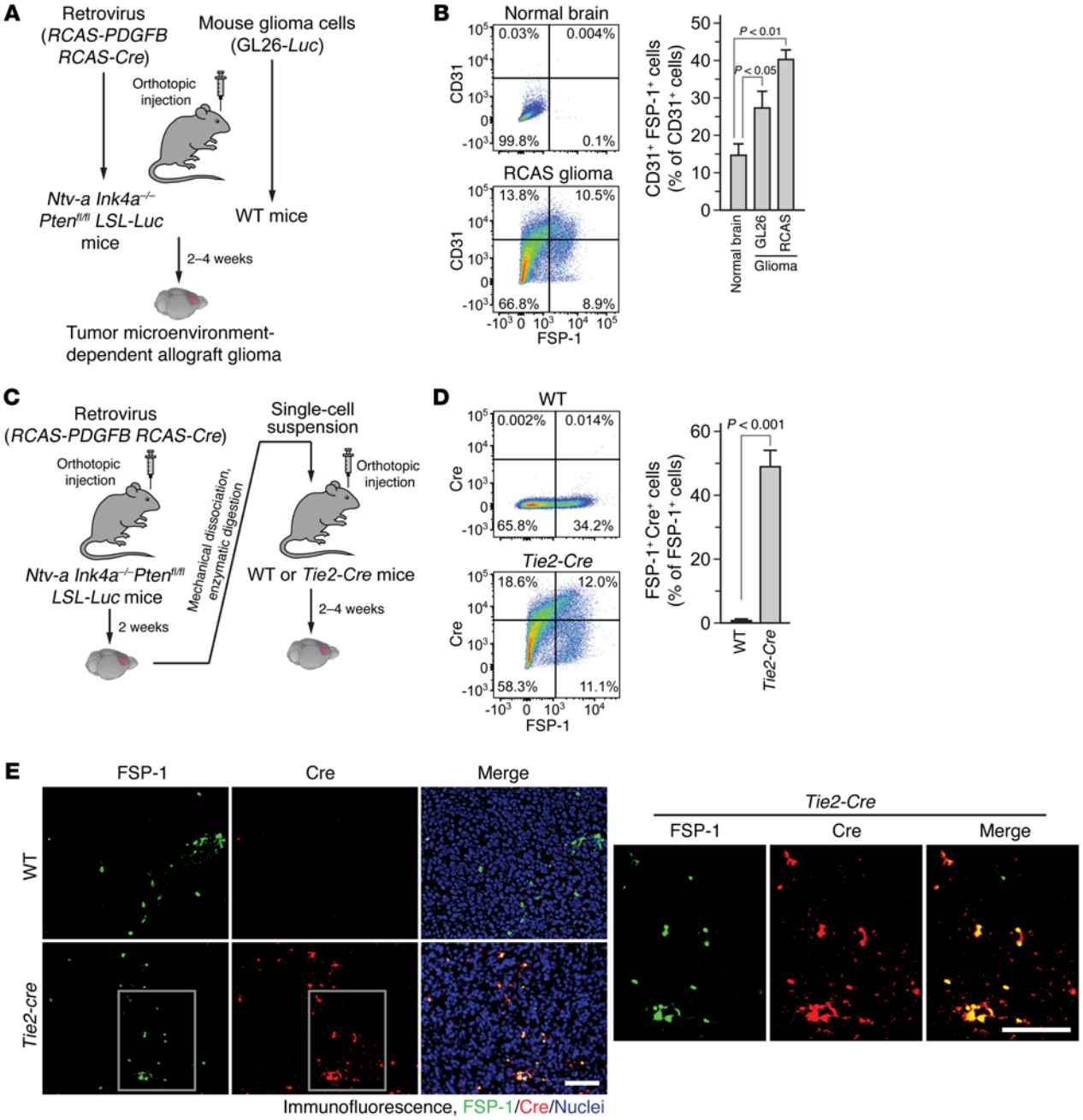

Figure 2. Robust Endo-MT in GBM vasculature. (**A** and **B**) GBM was induced by orthotopic injection of retrovirus or GL26 tumor cells. The GBM in *Ntv-a Ink4a*$^{-/-}$*Pten*$^{fl/fl}$ *LSL-Luc* mice is induced by PDGF overexpression and Cre-mediated *Pten* deletion in neural stem and progenitor cells through RCAS-mediated somatic gene transfer. (**A**) Schematic approach. (**B**) Single-cell suspension from normal brain and tumors was stained with anti-CD31 and anti–FSP-1 antibodies and analyzed by flow cytometry. Left, representative cell sorting. Right, quantitative analysis (mean ± SEM, n = 6–8, unpaired t test). (**C**–**E**) The primary GBM in *Ntv-a Ink4a*$^{-/-}$*Pten*$^{fl/fl}$ *LSL-Luc* donor mice is induced by RCAS-mediated somatic gene transfer. Recipient mice were WT and *Tie2-Cre* mice. (**C**) Schematic approach. (**D**) Single-cell suspensions derived from tumors were stained with anti-Cre and anti–FSP-1 antibodies and analyzed by flow cytometry. Left, representative cell sorting. Right, quantitative analysis (mean ± SEM, n = 6, unpaired t test). (**E**) Tumor sections were subjected to immunofluorescence analyses. Right, enlarged images of left rectangles. Representative data are shown from 4–5 mice. Scale bars: 100 μm.

of FSP-1 with EC markers CD105 and CD31 (Figure 1D), verifying mesenchymalization in human GBM-associated ECs.

To characterize the possible Endo-MT in vivo, we took advantage of 2 orthotopic, allogeneic murine glioma models with a native microenvironment, induced by RCAS/N-tva–mediated somatic PDGF gene transfer in *Ink4a*$^{-/-}$*Pten*$^{-/-}$ neural stem/progenitor cells and by injection of GL26 mouse glioma cells (Figure 2A). Notably, the transgenic GBM mouse model recapitulates the major features of human GBM, including prominent vascularity and vascular abnormality (23, 24). Flow cytometry analysis showed FSP-1 coexpression in about 30% and 40% of CD31^{+} EC in the GL26 and RCAS-induced tumors, respectively (Figure 2B).

Non-ECs including cancer cells may express CD31 during GBM progression (25, 26), which may contribute to the coexpression of

mesenchymal genes. To rule out this possibility and to specifically dissect the lineages of FSP-1$^+$ cells in the genetic GBM model, we utilized *Tie2-Cre* mice that express Cre under EC-specific promoter *Tie2* for EC lineage analysis (Figure 2C). Flow cytometry analysis with tumor single-cell suspension showed that about 50% of FSP-1$^+$ cells expressed Cre (Figure 2D), and Cre immunofluorescence with brain sections confirmed over half tumor-associated FSP-1$^+$ cells had EC origin (Figure 2E), suggesting a robust Endo-MT and its significant contribution to the generation of fibroblast-like cells in GBM. Database analysis of GBM gene expression reveals elevated *FSP1* mRNA in tumors, and high mRNA expression predicts poor glioma patient survival (Supplemental Figure 2), implicating a possible role of Endo-MT in glioma aggressiveness.

Additionally, previous work has shown that non-EC myeloid cells also express FSP-1 and Tie2 (27, 28), which may contribute to the tumor-associated FSP-1$^+$ cells derived from *Tie2-Cre*$^+$ lineage; however, our data showed a minimal coexpression of FSP-1 with myeloid marker CD11b and macrophage marker CD68 in human GBM (Supplemental Figure 3), implicating a minor role of myeloid cells in the detected Endo-MT. Furthermore, tumor-associated pericytes can also express Tie2 (28) and therefore may be detected by the *Tie2-Cre*–mediated lineage tracing in our mouse model. However, our data show that there was almost no coexpression of Cre with pericyte markers NG-2 in GL26 cell line tumors (Supplemental Figure 4), suggesting limited contributions of pericytes to *Tie2-Cre*$^+$ cells in GBM. In a parallel study, similar results were observed in RCAS-PDGF GBM tumor–bearing *Cdh5-Cre*^{ERT2} mice that express Cre under another EC-specific promoter *Cdh5* (not shown). These data confirm robust Endo-MT in GBM vasculature.

Endo-MT induces vascular abnormality in vitro. To verify GBM microenvironment–dependent Endo-MT, human brain microvascular ECs were treated with glioma conditioned medium (glioma-CM; collected from U251 or U87 cells and primary GBM cells cultured under hypoxia) in vitro. The treatment induced a cell morphology shift from the characteristic cobblestone appearance to fibroblast-like, spindle-shaped cells with disrupted distribution and reduced expression of endothelial-specific marker VE-cadherin (Figure 3A). Glioma-CM increased expression of mesenchymal markers FSP-1, N-cadherin, and α-SMA and decreased expression of endothelial markers VEGFR2 (Figure 3B). Similarly, FSP-1 expression was also induced by glioma-CM collected from different GBM cells including patient-derived primary tumor cells (Supplemental Figure 5). Consistently, coculture of ECs with different glioma cells induced N-cadherin and α-SMA expression and reduced VEGFR2 expression in ECs (Supplemental Figure 6). Furthermore, glioma-CM increased the mRNA expression of key mesenchymal genes including *HGF*, N-cadherin, and *FSP1*, as well as *SNAI2*, a transcriptional factor critical for mesenchymal transition, while decreasing the expression of endothelial-specific genes including *VEGFR2*, *CD146*, and *CD31* (Figure 3C). In addition, glioma-CM induced time-dependent expression of several transcriptional factors that may promote mesenchymal transition, including SNAI-2, ETS-1, and C/EBPβ (Supplemental Figure 7).

Strikingly, cells that were pretreated with the glioma-CM showed enhanced ability to proliferate, migrate, and invade (Figure 3D) with increased monolayer permeability (Figure 3E) and formed more abnormal vasculature with increased sprouting on Matrigel (Figure 3F) — even when cultured back in normal medium — suggesting that the tumor ECs are transformed to irreversibly acquire fibroblast characteristics including high proliferation, motility, and invasiveness. Likewise, GBM tumor–derived ECs showed increased ability to proliferate (Figure 3G). To rule out the possibility of contamination of other fast-growing cell types including pericytes in the GBM tumor– and normal brain–derived ECs, the cells were stained with anti–NG-2 antibody; however, no NG-2$^+$ cells were detected (not shown). In addition, glioma-CM treatment reduced expression of tight junction protein complex ZO-1, ZO-2, and CD2AP in ECs (Supplemental Figure 8), consistent with its hyperpermeability effects on EC monolayers.

Importantly, in contrast with previously characterized cell fate transition by Endo-MT, our data revealed that the transformed cells retained key functions of vascular EC, as shown by tube formation (Figure 3F) and EC-specific absorption of acetylated low-density lipoprotein (1,1'-dioctadecyl–3,3,3',3'-tetramethylindocarbocyanine perchlorate; Dil-Ac-LDL) (Figure 3H). These data suggest a major function of Endo-MT in vascular regulation during GBM progression, in contrast with its previously established role in de novo generation of fibroblasts.

c-Met induces Endo-MT and vascular abnormality. We then explored the molecular mechanisms underlying Endo-MT. Multiplex phospho-proteomic analysis identified EGFR and c-Met phosphorylation in glioma-CM–treated ECs (Figure 4A). Consistently, glioma-CM induced rapid phosphorylation of c-Met and EGFR at Tyr$^{1234/1235}$ and Tyr^{1068}, respectively, both essential for the kinase activation (Figure 4B). Pharmacological inhibitors of c-Met (SU11274) — and EGFR (erlotonib), to a lesser extent — remarkably suppressed glioma-CM–induced FSP-1 expression (Figure 4C). In addition, inhibition of TGF-β (by SB431542), a known mediator for EC differentiation and Endo-MT (14, 29), had a similar effect on FSP-1 expression. Moreover, HGF, the c-Met ligand, and TGF-β — but not EGF or VEGF-A — induced robust expression of FSP-1 and α-SMA (Figure 4D), and HGF blockage in glioma-CM by antibody neutralization substantially inhibited glioma-CM–induced FSP-1 and N-cadherin expression (Figure 4, E and F), suggesting that c-Met is required for Endo-MT. Furthermore, shRNA-mediated c-Met knockdown abrogated glioma-CM–induced FSP-1 and α-SMA expression (Figure 4G). Consistent with the critical role of c-Met in Endo-MT, HGF pretreatment, to a lesser extent than compared with glioma-CM, stimulates EC proliferation, migration, invasion, and tube formation (Supplemental Figure 9).

Further analyses indicated that c-Met is required for the enhanced abilities of ECs to proliferate and migrate (Figure 5, A and B), increased monolayer permeability (Figure 5C), and induced vessel abnormality on Matrigel including more dense tubes and sprout formation (Figure 5D), in response to glioma-CM pretreatment. Importantly, pharmacological c-Met inhibition normalized abnormal vessel formation in GBM tumor–derived ECs (Figure 5E). These findings establish a critical in vitro role of c-Met in Endo-MT and the subsequent abnormal vascularization.

c-Met phosphorylation induces ETS-dependent MMP-14 expression and VE-cadherin cleavage. Matrix metalloproteinases (MMPs) are fundamental to epithelial mesenchymal transition (EMT) (30). We investigated the role of MMPs in c-Met–mediated Endo-MT with a focus on those known to be induced by c-Met in ECs includ-

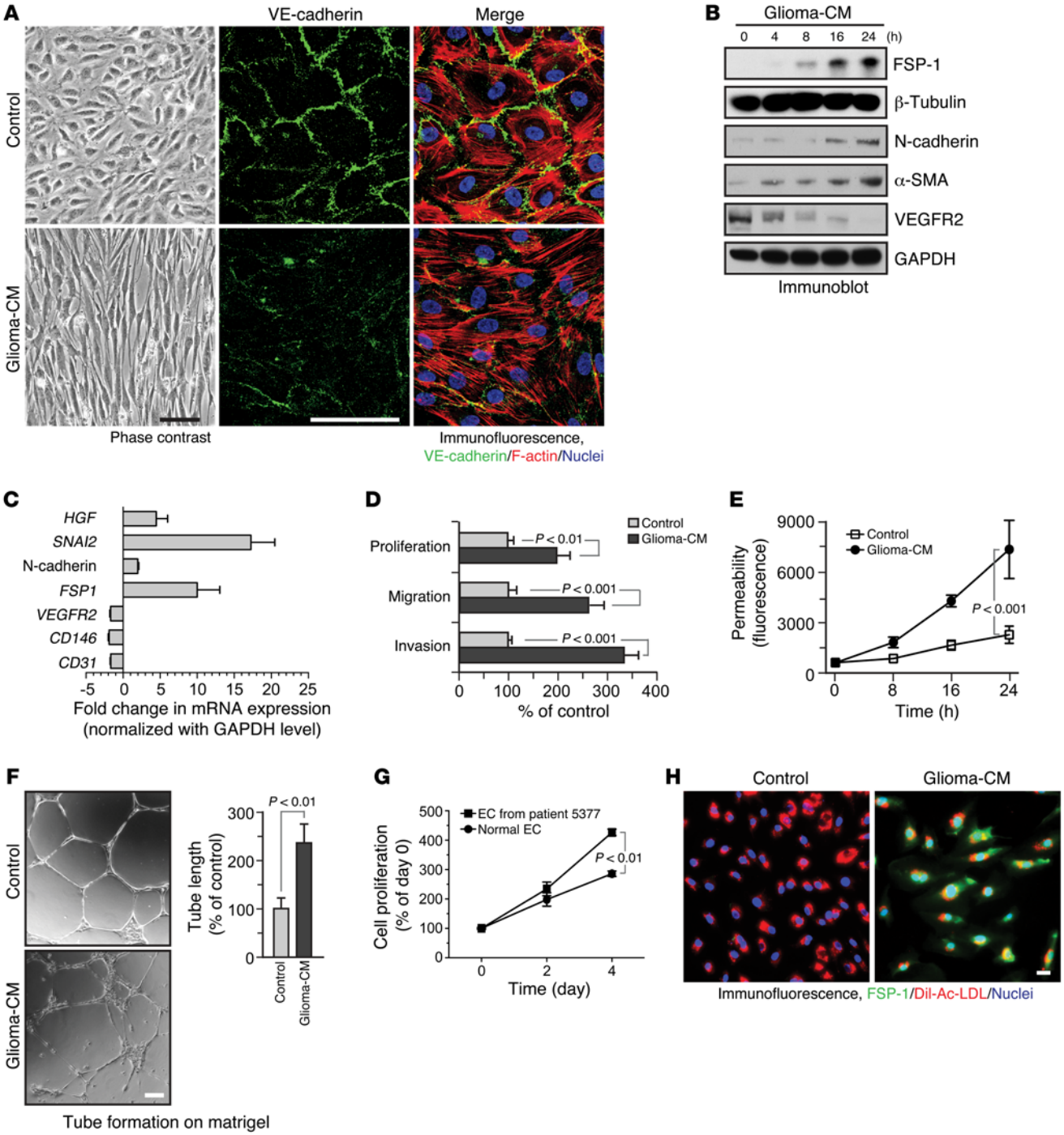

Figure 3. Endo-MT induces vascular abnormality in vitro. (**A**–**F**, and **H**) Human brain microvascular ECs were treated with control ECM or U251 glioma-CM. (**A**) Twenty-four hours after treatment, cells were stained with anti–VE-cadherin antibody and costained with Alexa Fluoro 567–labeled phalloidin for visualization of F-actin. Representative data are shown from 2 independent experiments. Scale bars: 100 μm. (**B**) ECs were lysed. Cell lysates were resolved by SDS-PAGE and immunoblotted. Representative data are shown from 3 independent experiments. (**C**) mRNA was isolated from ECs 24 hours after treatment and analyzed by qPCR (mean ± SEM, $n = 3$). (**D**–**F**) ECs pretreated with control medium or glioma-CM for 24 hours were trypsinized and cultured in normal culture medium. (**D**) Cell proliferation was determined with MTT assay. Cell migration was determined with transwell assay. Cell invasion across Matrigel-coated membranes in tranwells was determined. Data expressed as the percentage of control (mean ± SEM, $n = 5$, paired t test). (**E**) EC monolayer permeability was analyzed by measuring the fluorescence of diffused FITC-dextran across transwell membrane (mean ± SEM, $n = 6$, paired t test). (**F**) Tube formation was induced on Matrigel. Left, representative images. Right, quantified total tube length (mean ± SEM, $n = 6$, paired t test). Scale bar: 200 μm. (**G**) ECs isolated from normal brain or patient GBM tumor were subjected to cell viability analysis (mean ± SEM, $n = 4$, unpaired t test). (**H**) Cells pretreated with control medium or glioma-CM for 48 hours were incubated with DiI-Ac-LDL and stained with anti–FSP-1 antibody. Representative data are shown from 3 independent experiments. Scale bar: 50 μm.

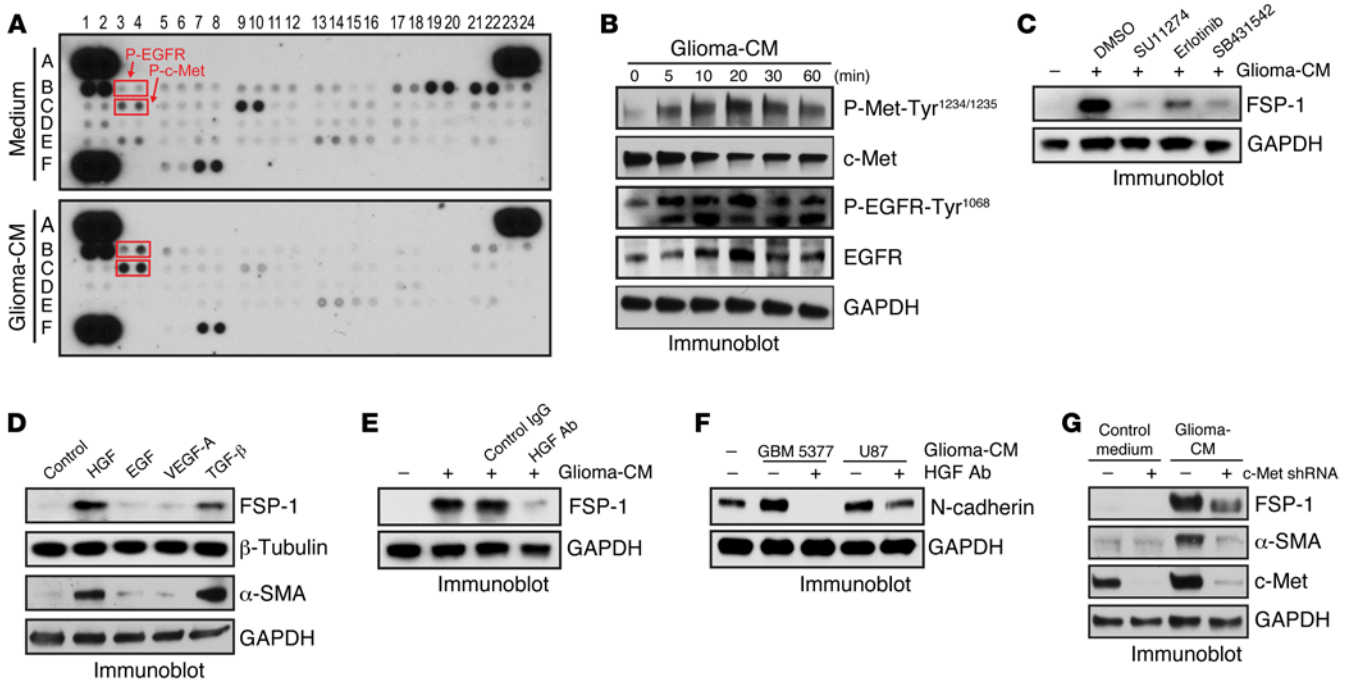

Figure 4. c-Met is a key regulator of Endo-MT. (**A**–**C**) Human brain microvascular ECs were treated with control ECM medium or U251 glioma-CM. (**A**) Cells were treated for 8 hours, and cell lysates were analyzed with a phospho-receptor tyrosine kinase array. (**B**) Cells were treated with glioma-CM for different time periods and subjected to immunoblot analysis. (**C**) Cells were treated with 5 μM c-Met inhibitor SU11274, EGFR inhibitor erlotinib, and TGF-β1 inhibitor SB431542 or 0.1% DMSO (vehicle) in glioma-CM for 24 hours and subjected to immunoblot analysis. (**D**) Cells were treated with 25 ng/ml HGF, 100 ng/ml EGF, 10 ng/ml VEGF-A, or 10 ng/ml TGF-β1 for 6 days. Cell lysates were analyzed by immunoblot. (**E** and **F**) Cells were treated with glioma-CM that was harvested from U251 (**E**), U87 (**F**), and primary patient 5377 GBM cells, in the presence of 20 μg/ml control IgG or anti-HGF antibody. Cell lysates were subjected to immunoblot analysis. (**G**) Cells transduced with control or c-Met shRNA were treated with control ECM medium and U251 glioma-CM for 24 hours. Cell lysates were analyzed by immunoblot. All representative blots are shown from 2–3 independent experiments.

ing MMP-1, -2, -14 (MT1-MMP) (31, 32). Glioma-CM selectively induced expression of MMP-14 but not MMP-1 and -2, while glioma-CM caused a slight, transient increased expression of MMP-2 at day 1 (Figure 6A). shRNA-mediated c-Met knockdown suppressed MMP-1, -2, and -14 expression in ECs with or without glioma-CM treatment (Figure 6B). However, shRNA targeting MMP-14, but not MMP-2, efficiently inhibited glioma-CM–induced FSP-1 and α-SMA expression (Figure 6, C and D), suggesting a critical role of c-Met–mediated MMP-14 expression in Endo-MT. To gain a molecular insight into the transcriptional regulation mechanism of MMP-14, we analyzed its promoter sequence and predicted that the transcriptional factors including activator protein-1 (AP-1), c-Jun, early growth response protein-1 (EGR-1), ETS-1, NF-κB, and serum response factor (SRF) may possibly bind to the region based on motif recognition pattern. Among this list of transcriptional regulators, NF-κB and ETS-1 are known to be activated by c-Met (31, 33). Immunofluorescence analysis verified HGF-induced activation of ETS and NF-κB in brain ECs, as indicated by their translocation from cytosol to nuclei (Supplemental Figure 10). Our data revealed that ETS-1 siRNA almost completely abolished HGF-induced expression of MMP-14 and FSP-1, while NF-κB siRNA only attenuated expression of FSP-1 but not MMP-14 (Figure 6E), suggesting that both transcriptional factors contribute to Endo-MT and that ETS-1 regulates Endo-MT through MMP-14 expression.

A hallmark of EMT is the downregulation of E-cadherin to reinforce the destabilization of adherent junctions (30). To examine the possibility that MMP-14 may cleave cell surface proteins that control adhesion and intercellular junctions, including VE-cadherin, ECs were incubated in vitro with purified, activated MMP-14. Immunoblot analysis identified a cleaved form of VE-cadherin (~100 kD) in the culture supernatant, accompanied by a decreased amount of its full-length form (~140 kD) in cells (Figure 6F); this suggested direct cleavage and degradation of VE-cadherin by MMP-14. Likewise, MMP-14 induced VE-cadherin disorganization and downregulation and increased FSP-1 expression in ECs (Figure 6, G and H). Furthermore, MMP-14 partially rescued FSP-1 expression in c-Met knockdown cells treated with glioma-CM (Figure 6H), suggesting a critical role of MMP-14 in c-Met–mediated Endo-MT. Likewise, MMP-14 expression was upregulated in GBM tumor–derived ECs while VE-cadherin expression was downregulated, compared with ECs isolated from normal brain (Figure 6I). Interestingly, c-Met inhibitor SU11274 increased VE-cadherin expression and decreased MMP-14 expression in GBM-associated ECs (Figure 6I), consistent with its effects on vessel normalization (Figure 5E). Together, these findings identify a molecular mechanism for Endo-MT, by which HGF activates c-Met and, in turn, induces ETS-1–dependent MMP-14 expression, thereby inducing VE-cadherin degradation and initiating Endo-MT.

c-Met drives Endo-MT, aberrant vascularization, and GBM progression and chemoresistance. To rigorously determine the role of c-Met in Endo-MT and GBM progression in vivo, we generated

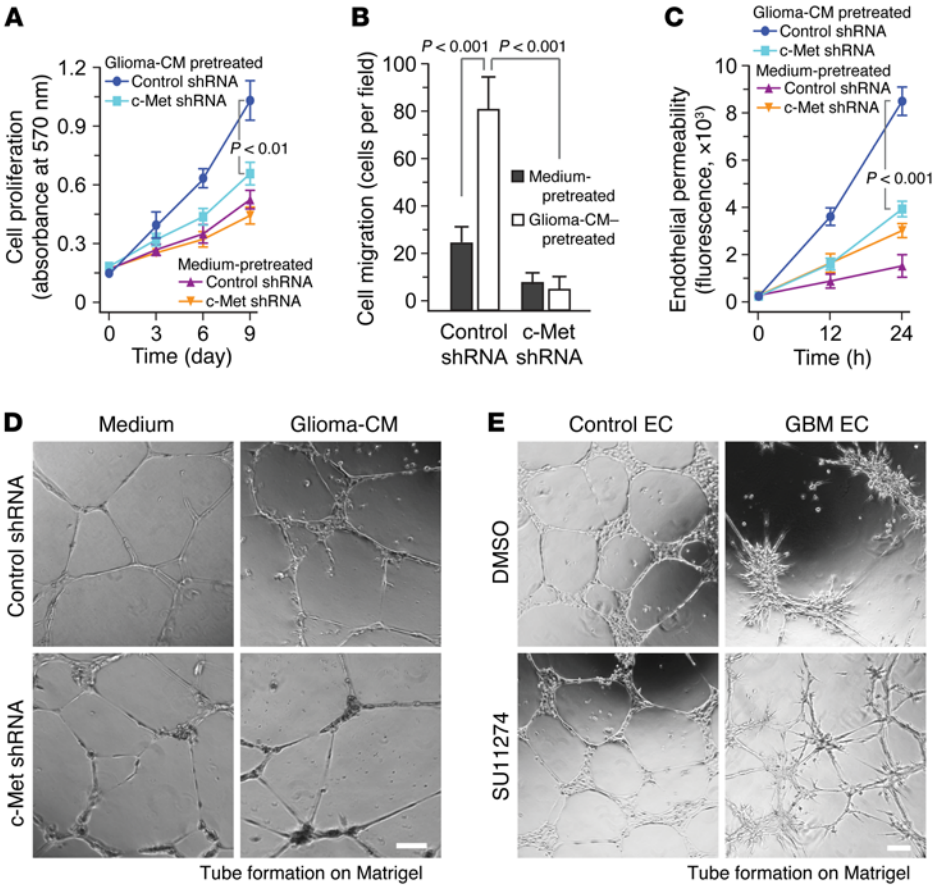

Figure 5. c-Met is required for glioma-CM–induced vascular abnormalities. (**A**–**D**) Human brain microvascular ECs were transduced with lentivirus that encodes control or c-Met shRNA and treated with control ECM medium and U251 glioma-CM for 24 hours. (**A**–**C**) After treatment, cells were trypsinized and cultured in normal medium. (**A**) Cell proliferation was determined by MTT-based assay (mean ± SEM, n = 6, paired t test). (**B**) Cells were seeded on transwell membranes and subjected to migration analysis (mean ± SEM, n = 6, paired t test). (**C**) EC monolayer permeability was analyzed by measuring the fluorescence of diffused FITC-dextran across transwell membrane (mean ± SEM, n = 6, paired t test). (**D**) Tube formation was induced on Matrigel. Representative data are shown from 3 independent experiments. Scale bar: 200 μm. (**E**) ECs isolated from normal human brain and GBM tumor of patient 5377 were pretreated with 5 μM SU11274 or 0.1% DMSO (vehicle). Tube formation was induced on Matrigel. Representative data are shown from 4 patients. Scale bar: 200 μm.

an EC-specific c-Met KO mouse line, *Tie2-Cre Met*$^{fl/fl}$, by crossing *Met*$^{fl/fl}$ mice with mice expressing Cre under EC-specific promoter *Tie2*. Interestingly, *Met* deletion in ECs did not affect basal angiogenesis, as indicated by apparently normal embryos with unaltered vascular density in the brain (Figure 7A) — in contrast with a previously well-established role of c-Met in pathological angiogenesis (34–36) — suggesting a dispensable role of c-Met in developmental angiogenesis. Immunoblot analysis with the ECs isolated from the mice verifies that *Met* KO inhibited the FSP-1 and MMP-14 expression induced by the glioma-CM (Figure 7B).

We then challenged these mice with an orthotopic injection of the tumor cells isolated from the RCAS-PDGF transgenic GBM model (Figure 7C). In the mice treated with saline, *Met* deletion in ECs did not alter animal survival (Figure 7D); similarly, *Met* deletion did not affect tumor growth in these mice (Figure 7E). However, in the mice treated with temozolomide (TMZ), *Met* deletion in ECs remarkably sensitized GBM tumors to TMZ treatment, as indicated by improved (+18 days) median survival in *Tie2-Cre Met*$^{fl/fl}$ mice, compared with an increase of 7.5 days in *Met*$^{fl/fl}$ mice (Figure 7D). Notably, about 20% of *Tie2-Cre Met*$^{fl/fl}$ mice survived for at least 60 days when the experiment was terminated, further suggesting the significance of this microenvironment-dependent mechanism of tumor resistance. Consistently, TMZ treatment robustly reduced tumor growth in *Tie2-Cre Met*$^{fl/fl}$, as evidenced by about a 70% decease in tumor volume, while there was a slight effect on control *Met*$^{fl/fl}$ mice (Figure 7E). Thus, EC-specific deletion of *Met* significantly overcomes GBM chemoresistance; in contrast, conventional anti-VEGF treatment does not improve patient survival or affect tumor resistance to radiation and chemotherapy (6).

Tumors from *Tie2-Cre Met*$^{fl/fl}$ mice showed markedly reduced vascular abnormality (Figure 7F). Tumor vessels of control *Met*$^{fl/fl}$ mice exhibited typical morphological features of vascular abnormality that is common in human GBM (i.e., they are tortuous and granular with extensive hemorrhage). Remarkably, the blood vessels in *Tie2-Cre Met*$^{fl/fl}$ mice appeared essentially normalized, as evidenced by nontortuous vessels with minimal hemorrhage and necrosis (Figure 7F). In addition, *Met* deletion in ECs inhibited hemorrhagic necrosis, a defining pathological feature of GBM. These data suggest that endothelial c-Met is critical for aberrant vascularization and GBM progression.

Furthermore, *Met* deletion in ECs inhibited FSP-1 and CD31 coexpression (Figure 8A), confirming its in vivo role in Endo-MT. Abnormal tumor vasculature is also characterized by insufficient coverage of nascent endothelium by pericytes, associated with poor functionality of the vasculature; vessel abnormalities induce plasma leakage, insufficient drug delivery, and spatially heterogeneous hypoxia, eventually leading to tumorigenesis and therapy resistance (1). *Met* deletion in ECs substantially increased the extent of pericyte coverage on tumor blood vessels (Figure 8B), inhibited the leakage of i.v. FITC-dextran (Figure 8C), and reduced intratumoral hypoxia (Figure 8D). Together, these results suggest that c-Met–mediated EC plasticity is critical for aberrant vascularization and therapeutic resistance in GBM.

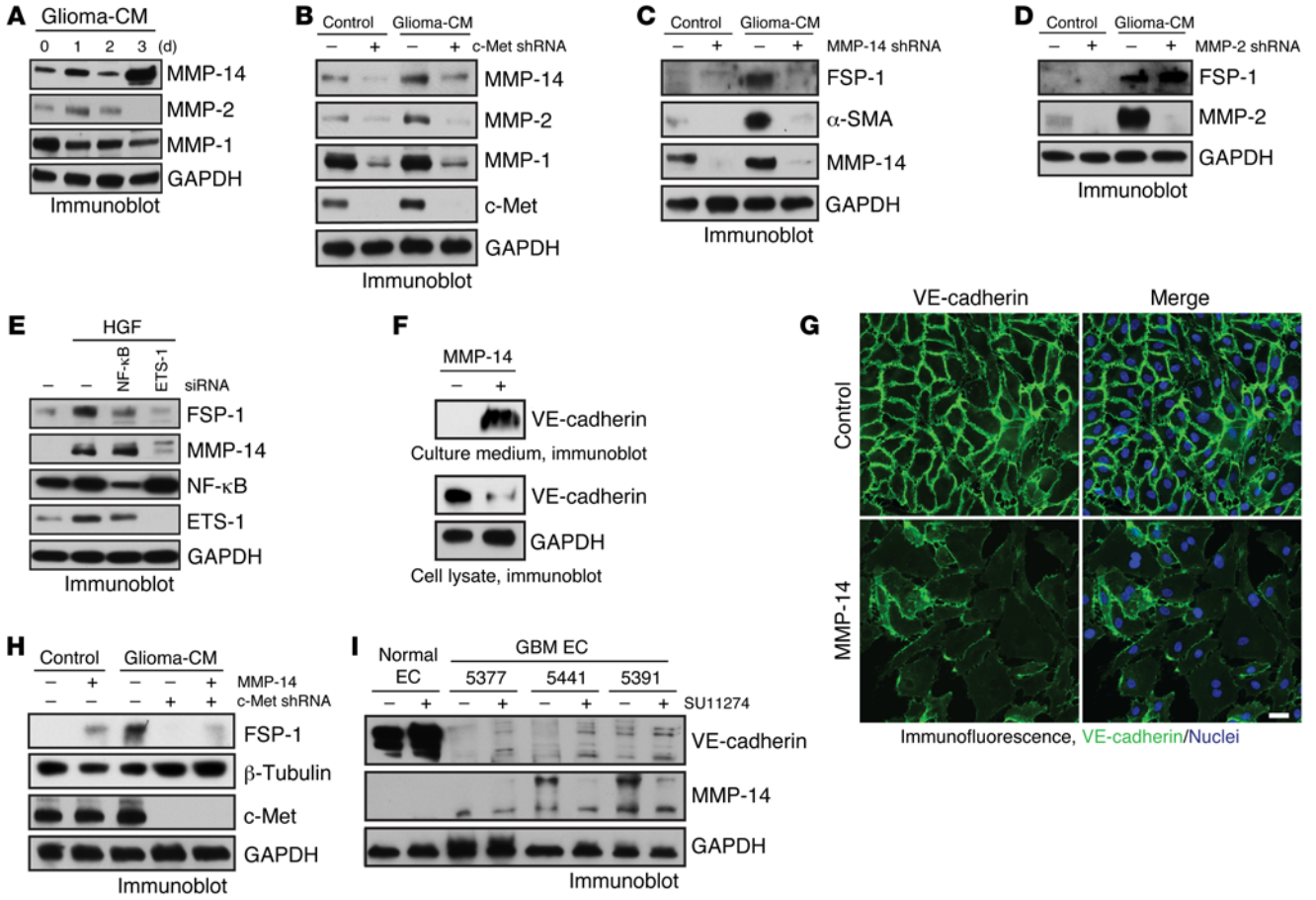

Figure 6. c-Met activation induces ETS-dependent MMP-14 expression, leading to VE-cadherin cleavage and Endo-MT. (**A**) Human brain microvascular ECs were treated with U251 glioma-CM and analyzed by immunoblot. (**B**) Cells were lentivirally transduced with c-Met or control shRNA and treated with glioma-CM. Cell lysates were subjected to immunoblot analysis. (**C** and **D**) Glioma-CM–induced FSP-1 or α-SMA expression is inhibited by knockdown of MMP-14 but not MMP-2. Cells transduced with MMP-14 (**C**), MMP-2 (**D**), or control shRNA were treated with glioma-CM and analyzed by immunoblot. (**E**) Cells were transfected with NF-κB, ETS-1, or control siRNA and treated with 100 ng/ml HGF. Cell lysates were subjected to immunoblot analysis. (**F** and **G**) Cells were incubated with active MMP-14 for 18 hours. (**F**) Culture medium and cell lysates were immunoblotted with anti–VE-cadherin antibody. (**G**) MMP-14 induces VE-cadherin disorganization and downregulation. Cells were subjected to immunofluorescence analysis with an anti–VE-cadherin antibody. Scale bar: 20 μm. (**H**) Cells were lentivirally transduced with c-Met or control shRNA, treated with glioma-CM in the presence or absence of active MMP-14, and analyzed by immunoblot. (**I**) ECs isolated from normal brain and patient GBM tumors were treated with 5 μM SU11274 or 0.1% DMSO (vehicle) and subjected to immunoblot analysis. All representative data are shown from 2–3 independent experiments.

Collectively, we show that HGF/c-Met activation induces Endo-MT in tumor-associated ECs, which in turn drives vascular abnormality by increasing cell proliferation, migration, and invasion, thereby inducing heterogeneous hypoxia and tumor resistance to treatment (Figure 9). We also identify a c-Met/ETS-1/MMP-14 axis, which induces VE-cadherin degradation and Endo-MT.

Discussion

Prominent vascularity and extreme vascular abnormality are hallmarks of cancer progression and treatment resistance in malignant tumors (3). However, conventional antiangiogenic therapies that target proangiogenic factors including VEGF-A have encountered difficulties and failures in treating some malignant tumors, including GBM (6), due to compensatory activation of other angiogenic factors, acquired treatment resistance, and other unidentified mechanisms. Here, we reveal that vascular transformation Endo-MT is a driving force for the excessive angiogenesis and vascular abnormality, by which tumor ECs acquire enhanced ability to sprout and outgrow, generating topologically and structurally abnormal vasculature that fuels tumor progression and induces chemoresistance in GBM. Additionally, our data reveal that GBM-associated ECs have diminished expression of VEGFR2, a major mediator of angiogenic VEGF signaling, providing a possible explanation for current ineffectiveness of anti-VEGF treatment in GBM. Consistently, glioma-CM pretreatment reduced EC response to B20 anti-VEGF antibody in cell proliferation, implying that Endo-MT confers resistance to anti-VEGF treatment (Supplemental Figure 11). Thus, targeting Endo-MT and EC transformative aberrations may provide new, promising strategies for vasculature-targeting therapy.

Cancer cells undergo robust genetic and epigenetic transformation, driving tumor initiation and progression, while the stromal cells, working as the supportive tissue, are considered genetically stable. However, previous studies have shown that tumor vas-

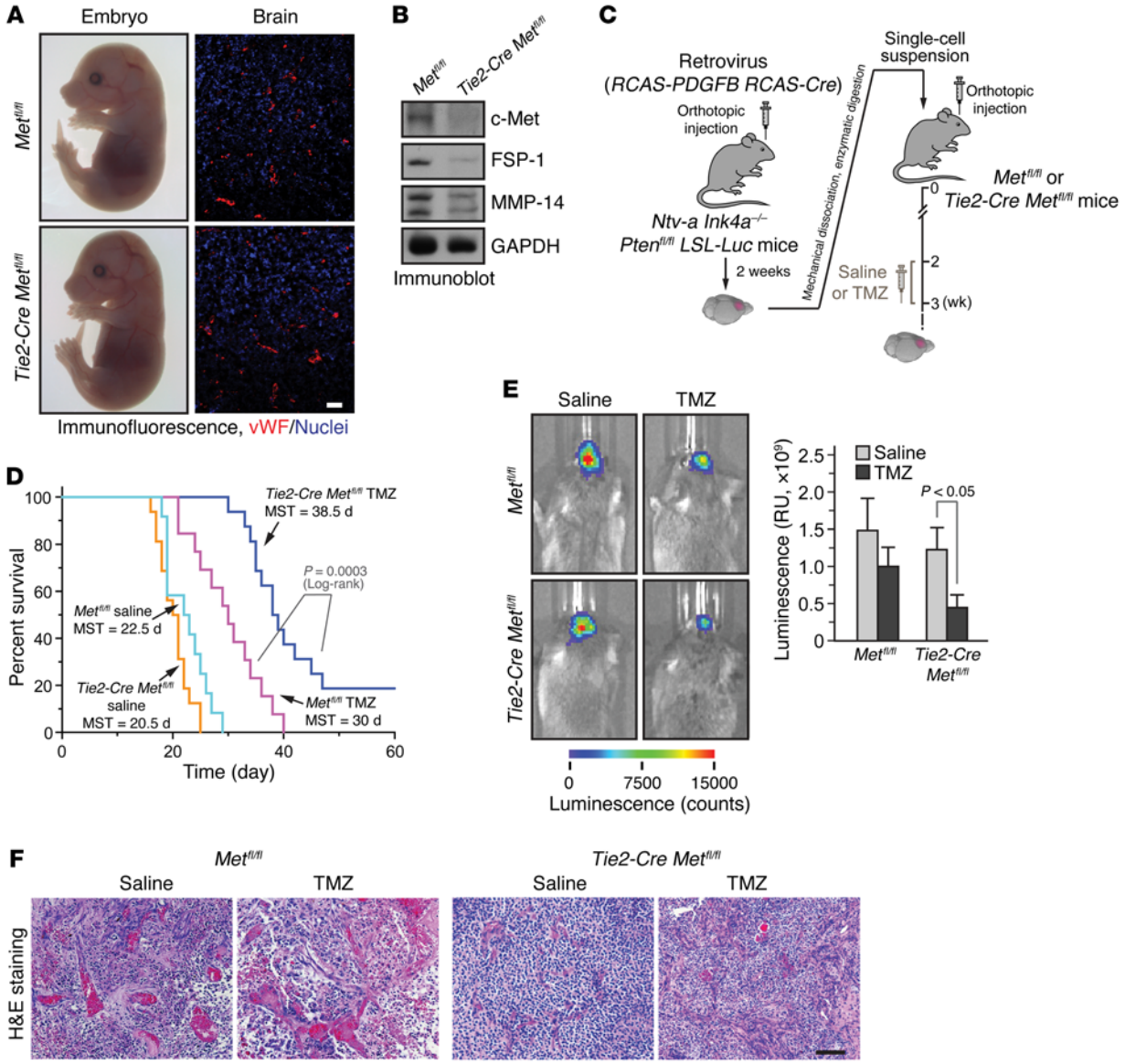

Figure 7. c-Met is critical for cancer progression and chemoresistance in GBM. (**A**) Angiogenesis analysis using *Met*$^{fl/fl}$ mice with or without expression of *Tie2-Cre*. Mouse embryos (left) at E14.5 were imaged, and brain tissues (right) were probed with anti-vWF antibody. Representative data are shown from 6 mouse embryos. Scale bar: 100 μm. (**B**) Aortic ECs were isolated from *Met*$^{fl/fl}$ and *Tie2-Cre Met*$^{fl/fl}$ mice and treated with GL26 glioma-CM. Cell lysates were immunoblotted. Representative data are shown from 2 independent experiments. (**C**–**F**) The genetic GBM model was induced. *Met*$^{fl/fl}$ and *Tie2-Cre Met*$^{fl/fl}$ mice were injected with primary GBM cells and treated with saline or 100 mg/kg TMZ 14 days after tumor transplantation. (**C**) Schematic model of experimental approaches. (**D**) Met deletion in ECs increases mouse survival with TMZ chemotherapy. Survival was monitored for 60 days after injection (total n = 57 mice, pooled from 2 independent experiments). MST, median survival time. (**E**) Met deletion in ECs inhibits tumor growth with TMZ chemotherapy. Tumor growth was analyzed by whole-body bioluminescence imaging. Left, representative images. Right, quantitative analysis of integrated luminescence in tumors at day 20 (n = 8–13, mean ± SEM, unpaired t test). (**F**) Tumor sections were stained with H&E and imaged. Representative data are shown from 8 mice/group. Scale bar: 100 μm.

culature also carries genetic alterations including chromosomal abnormalities (37–39). Particularly in GBM, ECs harbor the same genomic alterations as tumor cells, including chromosomal monosomy of the centromere of chromosome 10 (Cep10) and amplification of EGFR and chromosome 7 (Chr7) (40, 41), suggesting the genomic reprogramming of EC in tumor microenvironment. Robust EC transdifferentiation in embryonic development and pathological inflammatory settings further suggests a dynamic, instable genome in ECs. Therefore, similar to the cancer cell transformation that induces uncontrolled cell division, EC transformation, albeit not fully appreciated, is likely fundamental to vascular abnormality and tumorigenesis.

We characterize EC plasticity to acquire mesenchymal transformation (i.e., Endo-MT) in GBM tumor microenvironment. In contrast to its previously identified function for de novo generation of mesenchymal cells, we reveal that Endo-MT drives aberrant vascularization, in which EC acquires fibroblast phenotypes without the loss of endothelial functions. Importantly, the

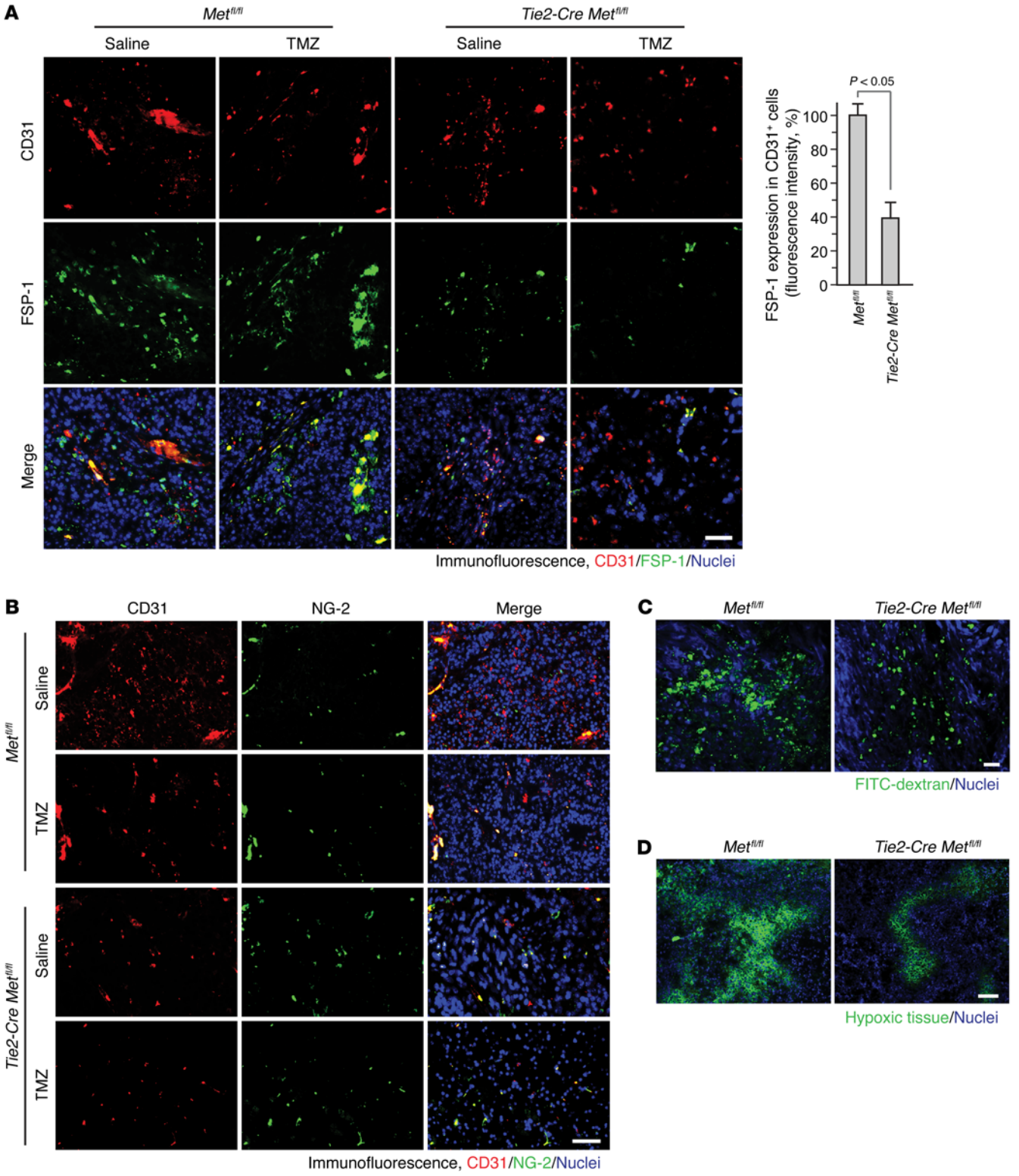

Figure 8. c-Met is critical for Endo-MT and aberrant vascularization in GBM. The genetic GBM model was induced in *Met*$^{fl/fl}$ and *Tie2-Cre Met*$^{fl/fl}$ mice and treated with saline or 100 mg/kg TMZ 14 days after tumor transplantation. (**A**) Tumor sections were probed with anti-CD31 and anti–FSP-1 antibodies. Representative data are shown from 5 mice/group. Scale bar: 100 μm. Right, FSP-1 fluorescence intensity in CD31$^+$ cells was quantified and expressed as percentage of the intensity in *Met*$^{fl/fl}$ mice treated with saline (n = 5, unpaired t test). (**B**) Tumor sections were fixed, probed with anti-CD31 and anti–NG-2 antibodies, and stained with Alexa Fluor 488– and 568–conjugated secondary IgGs (n = 3–5, representative data shown). Scale bar: 100 μm. (**C**) Mice were perfused i.v. with FITC-dextran. Tumors were excised, and the sections were imaged (n = 3–5, representative data shown). Scale bar: 50 μm. (**D**) Mice were injected with Hypoxyprobe-1 (pimonidazole HCl), and tumor sections were probed with antibody against pimonidazole adducts (n = 3–5, representative data shown). Scale bar: 100 μm.

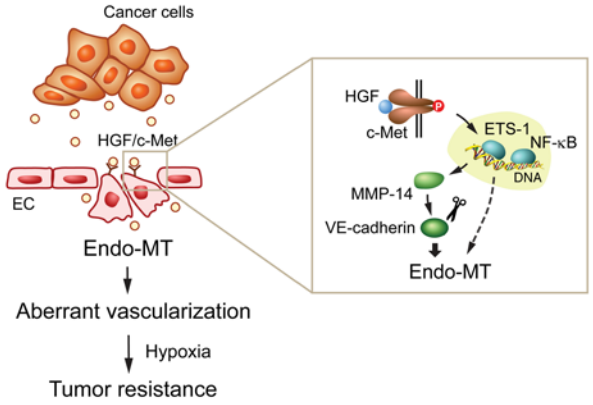

Figure 9. A schematic model. Cancer cell–derived HGF in the tumor microenvironment activates c-Met in EC, which in turn induces ETS-1–dependent MMP-14 expression, thereby inducing VE-cadherin cleavage and Endo-MT. Endo-MT generates abnormal vasculature and induces aberrant angiogenesis, leading to tumor progression and hypoxia-dependent tumor resistance.

expanded concept of EC transformation by our data probably provides a better explanation for the extensive vascularity observed in tumors, as previously characterized Endo-MT can theoretically decrease the EC population after complete cell transition.

Endo-MT is mediated through TGF-β, bone morphogenic protein (BMP), and Notch pathways (20, 42). Here we identify c-Met as a key regulator of EC plasticity and vessel abnormality. Consistently, c-Met inhibition significantly reduces tumor angiogenesis (35, 36). Interestingly, c-Met plays a role in EMT in tumor cells (43–45), but the precise mechanism remains largely unclear. We show that c-Met induces activation of ETS-1/MMP-14 to drive EC transformation, leading to vascular malformation and therapy resistance. Importantly, our data show that pharmacological inhibition of c-Met rescues MMP-14 and VE-cadherin dysexpression and abrogates vessel abnormalities in GBM-associated, patient-derived ECs, suggesting potential clinical application of c-Met inhibitors for vascular normalization.

In summary, our study reveals robust, c-Met–mediated EC plasticity to acquire mesenchymal transformation to promote EC proliferation and migration, causing aberrant vasculature and rendering chemoresistance in GBM. As such, targeted ablation of *Met* in ECs normalizes tumor vessels and significantly improves animal survival after chemotherapy, in contrast with ineffectiveness by current anti-VEGF therapies in GBM patients (6). Thus, EC plasticity may serve as an alternative target in antivascular and vessel normalization therapies, compared with conventional proangiogenic signaling pathways. Vascular detransformation may offer exciting opportunities to treat malignant cancer.

Methods

EC isolation from patient tumors. All patient samples were collected at the Department of Neurosurgery of the Hospital of the University of Pennsylvania (Supplemental Table 1). Tumor-derived single-cell suspensions were prepared by the tissue bank. Red cells were removed with ACK lysis buffer (Invitrogen). Cell suspension was subjected to magnetic activating cell sorting (MACS) with anti-CD31 antibody–conjugated magnetic beads (Miltenyi Biotec, catalog 130-091-935). Sorted ECs were verified by Dil-Ac-LDL (Alfa Aesar, catalog J65597) absorption, and 99% of cells were Dil-Ac-LDL$^+$.

Mice. *Tie2-Cre Met$^{fl/fl}$* mice were generated by crossing *Met$^{fl/fl}$* mice with*Tie2-Cre* mice (both from the Jackson Laboratory). Mice were genotyped with primers including Tie2-Cre (FP: 5′-GCGGTCTGG CAGTAAAAACTATC, RP: 5′-GTGAAACAGCATTGCTGTCACTT), Tie2-WT (FP: 5′-CTAGGCCACAGAATTGAAAGATCT, RP: 5′-GTAGGTGGAAATTCTAGCATCATCC), and Met (FP: 5′-TTAGGCAATGAGGTGTCCCAC, and RP: 5′-CCAGGTGGCTTCAAATTCTAAGG). *Cdh5-Cre^{ERT2}* mice were generated by Ralf Adams (Max Planck Institute for Molecular Biomedicine, Münster, Germany) and provided by Bisen Ding (Cornell University, New York City, New York, USA) (46). All animals were housed in the Association for the Assessment and Accreditation of Laboratory Animal Care–accredited animal facility of the University of Pennsylvania.

GBM mouse model. GBM was induced in mice previously described (24, 47, 48). In brief, chicken DF-1 fibroblasts (ATCC) were transfected with RCAS-PDGF-B and RCAS-Cre plasmids to produce retrovirus and orthotopically injected into *Ntv-a Ink4a$^{-/-}$Pten$^{fl/fl}$ LSL-luc* mice (kindly provided by Eric Holland, Fred Hutchinson Cancer Research Center, Seattle, Washington) to induce GBM through RCAS/n-tva–mediated gene transfer. Tumors were isolated and subjected to mechanical dissociation with a gentleMACS Dissociator (Miltenyi Biotec) and enzymatic digestion with collagenase II and dispase II to obtain single-cell suspensions. About 8-week-old *Met$^{fl/fl}$*, *Tie2-Cre Met$^{fl/fl}$*, and *Tie2-Cre* mice (half male and half female) were orthotopically, stereotactically injected with 10^5 GBM tumor cells or GL26 mouse glioma cells that expressed luciferase. Tumor growth was monitored by whole-body bioluminescence using an IVIS 200 Spectrum Imaging System after retro-orbital injection of luciferin (150 mg/kg, Gold Biotechnology). Mice were administrated with peritoneal injection of saline or 100 mg/kg TMZ (SelleckChem) 2 weeks after GBM induction. Postinjection survival was monitored for 60 days. Mice were euthanized when exhibiting severe GBM symptoms including domehead, hemiparesis, or more than 20% body weight loss.

Tumor vessel perfusion assay. Tumor-bearing mice were retro-orbitally injected with FITC-labeled dextran (100 mg/kg, Santa Cruz Biotechnology Inc.). After 20 minutes, the mice were perfused through the left ventricle with PBS, and tumors were collected after mice were euthanized. Cryostat sections were mounted with DAPI and imaged with an Eclipse TE2000-U fluorescence microscope (Nikon) equipped with a Retiga 2000R CCD camera (QImaging).

Analysis of tumor hypoxia. Tumor hypoxia was determined with Hypoxyprobe-1 Plus Kit (Hypoxyprobe). Mice were i.v. injected with pimonidazole-HCl (60 mg/kg). Tumor-frozen sections were fixed with chilled acetone and stained with antipimonidazole adduct FITC-conjugated antibody following manufacture instructions. Images were acquired with the fluorescence microscope.

Immunofluorescence and histology. Human surgical and biopsy specimens from subjects with GBM (US Biomax and BioChain), or normal brain tissues, were deparaffinized, rehydrated, and subjected to antigen retrieval in Target Retrieve Solution (Dako, catalog S1699) at 95°C for 20 minutes. Sections were blocked with 5% horse serum for 1 hour at room temperature, incubated with anti-CD31 (1:100, Dako, catalog M0823), anti-CD105 (1:100, Dako, catalog M3527), anti-FSP-1 (1:100, Dako, catalog A5114), anti-CD11b (1:100, BioLegend, catalog 301311),

anti-CD68 (1:100, BD Biosciences, catalog 556059), anti–P-Met-Tyr$^{1234/1235}$ (1:100, Cell Signaling Technology, catalog 3077), and anti–P-Met-Tyr^{1349} (1:100, Cell Signaling Technology, catalog 3133) antibodies overnight at 4°C. For mouse tissues, frozen sections were fixed with chilled acetone for 20 minutes and blocked with 2% horse serum for 1 hour at room temperature. Paraffin sections were deparaffinized and rehydrated, subjected to antigen retrieval in Target Retrieve Solution at 95°C for 20 minutes, and blocked with 5% horse serum for 1 hour at room temperature. Sections were incubated with anti-Cre (1:100, Millipore, catalog MAB3120), anti-vWF (1:100, Dako, catalog A0082), and anti–NG-2 (1:100, Millipore, catalog AB5320) antibodies overnight at 4°C. For histological study, sections were stained with H&E and imaged with an AxioLab microscope (Zeiss) equipped with an AxioCam HRC CCD camera (Zeiss). Cultured cells were fixed with 4% paraformaldehyde for 20 minutes and incubated with anti–VE-cadherin (1:100, Cell Signaling Technology, catalog 2500) and anti–α-SMA (1:100, Abcam, catalog ab5694). Sections were stained with Alexa Fluor 488– and 568–conjugated secondary IgGs (1:500, Invitrogen) for 1 hour at room temperature. Images were acquired with the fluorescence microscope.

Preparation of glioma cell–conditioned medium. Human U251 and U87 glioma cells and primary patient glioma cells and mouse GL26 glioma cells were cultured with DMEM medium supplemented with 5% FBS. Cells at about 90% confluence were exposed to hypoxia (1% O_2) in a humidified air atmosphere at 37°C for 24 hours. Culture medium were centrifuged at 5,000 × *g* for 30 minutes to remove cellular debris, and the supernatant collected.

Cell culture and treatment. Human brain microvascular ECs (ScienCell Research Laboratories and PromoCell) were maintained in EC Medium (ECM, ScienCell Research Laboratories). All cells were used between passages 2 and 5. Cells were treated with recombinant human HGF (25 ng/ml, PeproTech, catalog 100-39), EGF (100 ng/ml, PeproTech, catalog AF-100-15), VEGF (10 ng/ml, PeproTech, catalog 100-20), TGF-β1 (10 ng/ml, PeproTech, catalog 100-21C), c-Met inhibitor SU11274 (5 μM, SelleckChem, catalog S1080), EGFR inhibitor erlotinib (5 μM, SelleckChem, catalog S1023), TGF-β1 inhibitor SB431542 (5 μM, SelleckChem, catalog S1067), or glioma-CM neutralized with 20 μg/ml control rabbit IgG (Cell Signaling Technology, catalog 2729), anti-HGF antibody (R&D Systems, catalog AB-294-NA), or anti-VEGF antibody (Genentech, catalog B20).

quantitative PCR analysis. mRNA was isolated with an RNeasy Mini Kit (QIAGEN) and subjected to quantitative PCR (qPCR) with SuperScript III First-Strand Synthesis SuperMix (Invitrogen). qPCR was performed in a 25-μl reaction volume using Fast SYBR Green Master Mix (Applied Biosystems) and primers: *HGF* (FP: 5′-TTCAAGTGCAAGGACCTACG-3′, RP: 5′-GTTTGGAATTTGGGAGCAGT-3′), *SNAI2* (FP: 5′-ACAGAGCATTTGCAGACAGG-3′, RP: 5′-GTGCTACACAGCAGCCAGAT-3′), N-cadherin (FP: 5′-CCTGCTTATCCTTGTGCTGA-3′, RP: 5′-CCTGGTCTTCTTCTCCTCCA-3′), *FSP1* (FP: 5′-TCTCTCCTCAGCGCTTCTTC-3′, RP: 5′-AACTTGTCACCCTCTTTGCC-3′), *VEGFR2* (FP: 5′-CTCGGGTCCATTTCAAATCT-3′, RP: 5′-GCTGTCCCAGGAAATTCTGT-3′), *CD146* (FP: 5′-GAGGAGGTCGCTACCTGTGT-3′, RP: 5′-CCAGCTGTGCCTTCAGAATA-3′), *CD31* (FP: 5′-ACTGTGCCTGCAGTCTTCAC-3′, RP: 5′-TGAACAGAGCAGAAGGGTCA-3′), *CEBPB* (FP: 5′-GCAACCCACGTGTAACTGTC-3′, RP: 5′-AACAAGCCCGTAGGAACATC-3′), *STAT3* (FP: 5′-AGGAGGCGTCACTTTCACTT-3′, RP: 5′-GCTGCTGCTTTGTGTATGGT-3′), *FOSL2* (FP: 5′-ATGAGCAGCTGTCTCCTGAA-3′, RP: 5′-CCTGACTTCTCCTCCTCCAG-3′), *RUNX1* (FP: 5′-GGACGAATCACACTGAATGC-3′, RP: 5′-TGTGGGTACGAAGGAAATGA-3′), *ETS1* (FP: 5′-AGTGAGGTGCTGAGAGCAGA-3′, RP: 5′-GTGTTGCTAGGTCCTTGCCT-3′), and *NFKB1* (FP: 5′-GTGCAGAGGAAACGTCAGAA-3′, RP: 5′-TGGGAAGCTATACCCTGGAC-3′).

Phospho-RTK array. ECs were treated with control medium and glioma-CM for 8 hours. Cell lysates were analyzed with a Proteome Profiler Human Phospho-RTK Array Kit (R&D Systems, catalog ARY001B) following manufacture instructions.

Isolation and culture of mouse ECs. Thoracic aorta was isolated from 3-week-old mice and cut into pieces. Aortic rings were embedded in Matrigel-coated dishes incubated in culture medium with 5% FBS for 5 days. After rinsing with PBS, the rings were removed, and remaining cells incubated with 2 U/ml Dispase I (GIBCO, ThermoFischer Scientific; catalog 17105-041) for 20 minutes at 37°C. After centrifugation at 500 × *g* for 10 minutes, the cell pellets were washed with PBS, and cells were cultured in DMEM/F-12 medium supplemented with 25 mg/ml EC growth supplement (Sigma-Aldrich) and 5% FBS at 37°C in a humidified air atmosphere with 5% CO_2. All cells were used between passages 2 and 4.

Dil-Ac-LDL absorption assay. ECs cultured in 8-well chamber slides (Falcon, catalog 354108) at 70% confluence were treated with control medium or glioma-CM for 48 hours. After washing with PBS, cells were incubated with Dil-Ac-LDL (10 μg/ml, Alfa Aesar, catalog J65597) in serum-free medium containing 3% BSA for 5 hours at 37°C. Cells were washed, fixed with 3% paraformaldehyde, and stained with anti–FSP-1 antibody (1:100, Dako, catalog A5114) and Alexa Fluor 488–conjugated IgG. The slides were mounted with DAPI-containing mounting medium (Vector Laboratories, catalog H-1200). Images were acquired with the fluorescence microscope.

In vitro tube formation assay. Growth factor–reduced Matrigel (120 μl/chamber, Corning Inc., 356231) was added to 8-chamber culture slides, incubated at 37°C for 20 minutes, and washed with PBS. ECs were pretreated with glioma-CM or control medium for 24 hours and trypsinized and seeded on Matrigel at a density of 2×10^4 cells/chamber. Cells were imaged with an Axiovert 40CFL inverted microscope (Zeiss) equipped with AxioCam MRM CCD camera (Zeiss).

Cell proliferation assay. EC pretreated with glioma-CM or control medium were trypsinized and seeded on 96-well plates at a density of 7,500 cells/well, and allowed to attach for 4 hours. Cell proliferation was determined by MTT assay (24). Absorbance was measured at 570 nm with a reference at 620 nm in a Spectramax 190 spectrophotometer (Molecular Devices).

Cell viability assay. ECs pretreated with glioma-CM or control medium were trypsinized and seeded on 96-well plates at a density of 7,500 cells/well and allowed to attach for 4 hours. Cell viability was determined by Cell-Titer assay (Promega, catalog G7571) according to the manufacturer's instruction. Luminescence was detected by using a luminescent plate reader (Synergy H4 Hybrid, BioTek).

In vitro vascular permeability assay. ECs pretreated with glioma-CM or control medium were seeded on Transwell inserts with 0.4 μm pore membrane (CoStar, catalog 3412) in 6-well plates, allowed to attach for 4 hours, and cultured for 3 days to reach confluence. Cells were incubated with control medium or glioma-CM without Phenol Red. FITC-dextran (MW = 70,000 Da, 10 μg/ml, Santa Cruz Biotechnology Inc., catalog sc-263323) was added to the top chamber. The medium from the lower chamber was collected, and fluo-

rescence was measured with excitation wavelength at 485 nm and emission at 530 nm.

Cell migration and invasion assays. ECs were seeded 2×10^4 cells/well on 8 μm–pore insert membranes (Falcon, catalog 353097) precoated with (for invasion assay) or without (for migration assay) Matrigel in a 24-well plate and allowed to attach for 4 hours. Cell migration was induced by adding 5% FBS in the bottom chamber. After a 6-hour induction, cells on the top of membrane were swiped off with cotton swab. Cells were fixed in methanol for 5 minutes and stained with Toluidine Blue O (Sigma-Aldrich, catalog 198161) for 5 minutes. Images were taken in 3–4 fields per well, and stained cells were counted.

siRNA and shRNA treatment. ECs at 50% confluence were transfected with nontargeting control siRNA (QIAGEN, catalog 1027280) or siRNA targeting c-Met (Cell Signaling Technology, catalog 6618), MMP-2 (Invitrogen, catalog s8851), MMP-14 (Invitrogen, catalog s8877), NF-κB (Cell Signaling Technology, catalog 8242), and ETS-1 (Cell Signaling Technology, catalog 6258) using Lipofectamine 2000 (Invitrogen, catalog 11668-019) in serum-free Opti-MEM medium (GIBCO, ThermoFischer Scientific; catalog 31985-070) for 12 hours, followed by recovery with serum-supplemented medium for 24 hours. Alternatively, ECs were transduced with lentivirus encoding shRNA targeting c-Met (Sigma-Aldrich, catalog TRCN0000121248), MMP-2 (Sigma-Aldrich, catalog TRCN0000290300), MMP-14 (Sigma-Aldrich, catalog TRCN0000429314), or scrambled sequence (Sigma-Aldrich, catalog SHC016V-1EA) with 8 μg/ml polybrene (Millipore, catalog TR-1003-G) for 24 hours, followed by recovery with serum-supplemented medium for 24 hours.

MMP-14 activation and treatment. Recombinant human MMP-14 (40 μg/ml, R&D Systems, catalog 918-MP-010) was activated with 0.86 μg/ml rhFurin (R&D Systems, catalog 1503-SE-010) in activation buffer (50 mM Tris buffer [pH9.0], 1 mM $CaCl_2$, and 0.5% Brij-35) for 1.5 hours at 37°C. ECs were treated with active MMP-14 in ECM medium supplemented with 3 mM $CaCl_2$ and 1 μM $ZnCl_2$ for 18 hours at 37°C. Cell culture medium was collected and centrifuged at 5,000 × *g* for 2 minutes at 4°C to remove cell debris. Cell lysates and medium supernatant were immunoblotted with anti–VE-cadherin (1:1,000, Enzo, catalog ALX-210-232-C100) and anti-GAPDH (1:1,000, Cell Signaling Technology, catalog 5174) antibodies.

Immunoblot analysis. Cells were lysed with an NP-40 buffer containing protease inhibitor cocktail (Roche Diagnostics, catalog 11697498001), followed by measurement of total protein concentration. Protein (20 μg) was resolved by 4%–15% precast SDS-PAGE gel (Bio-Rad). After transfer, PVDF membranes were blotted with anti-GAPDH (Cell Signaling Technology, catalog 5174), anti–FSP-1 (Millipore, catalog 07-2274, and Abcam, catalog ab27957), anti-Tie2 (Cell Signaling Technology, catalog 4224), anti-VEGFR2 (GenScript, catalog a00357), anti–N-cadherin (Cell Signaling Technology, catalog 13116), anti–α-SMA (Abcam, catalog ab5694), anti–c-Met (Cell Signaling Technology, 8198), anti-EGFR (Cell Signaling Technology, 2232), anti–P-Met$^{1234/1235}$ (Cell Signaling Technology, catalog 3077), anti–P-EGFR-Tyr^{1068} (Cell Signaling Technology, catalog 3777), anti–MMP-1 (Biomal, catalog SA-102), anti–MMP-2 (Cell Signaling Technology, catalog 4022), anti–MMP-14 (Cell Signaling Technology, catalog 13130), anti–NF-κB (Cell Signaling Technology, catalog 8242), anti–ETS-1 (Cell Signaling Technology, catalog 6258), and anti-CD2AP (Cell Signaling Technology, catalog 2135), anti–ZO-1 (Cell Signaling Technology, catalog 8193), and anti–ZO-2 (Cell Signaling Technology, catalog 2847) antibodies at 1:1,000 dilutions. Proteins were detected with HRP-conjugated antibodies specific for either rabbit or mouse IgG (Bio-Rad), followed by ECL development (GE Healthcare, catalog RPN2232).

Statistics. Student's *t* test and LogRank analysis (Prism) were used for statistical analysis between groups, and *P* values less than 0.05 were considered statistically significant.

Study approval. All experiments with mice were performed in accordance with a protocol approved by the Institutional Animal Care and Use Committee of the University of Pennsylvania and with the NIH *Guide for the Care and Use of Laboratory Animals* (8th ed. The National Academies Press. 2011). The collection of human tissues in compliance with the tissue banking protocol was approved by the University of Pennsylvania IRB, and written informed consent was obtained from each participant.

Author contributions

MH designed, performed, and analyzed experiments; produced figures; and wrote the initial draft of the paper. PM, RAM, and PC contributed to immunofluorescence analysis. LR, DMO, and ND prepared single-cell suspensions of glioma specimens. TL, ZZ, HJK, EY, DZ, CL, LZ, BZ, YG, and CK provided helpful suggestions for designing experiments. YF designed, supervised, and analyzed experiments and wrote the final draft of the manuscript. All authors commented on the manuscript.

Acknowledgments

We are grateful to Eric Holland and Ralf Adams for providing the RCAS-PDGF GBM model and *Cdh5-Cre^{ERT2}* mice, respectively, and to Celeste Simon, Brian Keith, and Sandra Ryoem for helpful discussions. This work was supported in part by NIH grants R00 HL103792, R01 NS094533 (both to Y. Fan), and R01 CA190415 (to L. Zhang); American Heart Association Scientist Development Grant SDG9050018 (to Y. Gong); University of Pennsylvanian Academic Development Fund (to Y. Fan); Abramson Cancer Center Neuro-oncology Innovation Award (to Y. Fan); and McCabe Award (to Y. Fan).

Address correspondence to: Yi Fan, Department of Radiation Oncology, University of Pennsylvania Perelman School of Medicine, 3400 Civic Center Blvd, SCTR 8-132, Philadelphia, Pennsylvania 19104, USA. Phone: 215.898.9291; E-mail: fanyi@uphs.upenn.edu.

1. Carmeliet P, Jain RK. Principles and mechanisms of vessel normalization for cancer and other angiogenic diseases. *Nat Rev Drug Discov*. 2011;10(6):417–427.
2. Weis SM, Cheresh DA. Tumor angiogenesis: molecular pathways and therapeutic targets. *Nat Med*. 2011;17(11):1359–1370.
3. Hanahan D, Weinberg RA. Hallmarks of cancer: the next generation. *Cell*. 2011;144(5):646–674.
4. Stupp R, et al. Radiotherapy plus concomitant and adjuvant temozolomide for glioblastoma. *N Engl J Med*. 2005;352(10):987–996.
5. Huse JT, Holland EC. Targeting brain cancer: advances in the molecular pathology of malignant glioma and medulloblastoma. *Nat Rev Cancer*. 2010;10(5):319–331.
6. Gilbert MR, et al. A randomized trial of bevacizumab for newly diagnosed glioblastoma. *N Engl J Med*. 2014;370(8):699–708.
7. Batchelor TT, et al. AZD2171, a pan-VEGF receptor tyrosine kinase inhibitor, normalizes tumor

vasculature and alleviates edema in glioblastoma patients. *Cancer Cell*. 2007;11(1):83–95.
8. Kovacic JC, Mercader N, Torres M, Boehm M, Fuster V. Epithelial-to-mesenchymal and endothelial-to-mesenchymal transition: from cardiovascular development to disease. *Circulation*. 2012;125(14):1795–1808.
9. Eilken HM, Nishikawa S, Schroeder T. Continuous single-cell imaging of blood generation from haemogenic endothelium. *Nature*. 2009;457(7231):896–900.
10. Boisset JC, van Cappellen W, Andrieu-Soler C, Galjart N, Dzierzak E, Robin C. In vivo imaging of haematopoietic cells emerging from the mouse aortic endothelium. *Nature*. 2010;464(7285):116–120.
11. Kissa K, Herbomel P. Blood stem cells emerge from aortic endothelium by a novel type of cell transition. *Nature*. 2010;464(7285):112–115.
12. Bertrand JY, Chi NC, Santoso B, Teng S, Stainier DY, Traver D. Haematopoietic stem cells derive directly from aortic endothelium during development. *Nature*. 2010;464(7285):108–111.
13. Lancrin C, Sroczynska P, Stephenson C, Allen T, Kouskoff V, Lacaud G. The haemangioblast generates haematopoietic cells through a haemogenic endothelium stage. *Nature*. 2009;457(7231):892–895.
14. Zeisberg EM, et al. Endothelial-to-mesenchymal transition contributes to cardiac fibrosis. *Nat Med*. 2007;13(8):952–961.
15. Li J, Qu X, Bertram JF. Endothelial-myofibroblast transition contributes to the early development of diabetic renal interstitial fibrosis in streptozotocin-induced diabetic mice. *Am J Pathol*. 2009;175(4):1380–1388.
16. Zeisberg EM, Potenta SE, Sugimoto H, Zeisberg M, Kalluri R. Fibroblasts in kidney fibrosis emerge via endothelial-to-mesenchymal transition. *J Am Soc Nephrol*. 2008;19(12):2282–2287.
17. Medici D, Shore EM, Lounev VY, Kaplan FS, Kalluri R, Olsen BR. Conversion of vascular endothelial cells into multipotent stem-like cells. *Nat Med*. 2010;16(12):1400–1406.
18. Chen PY, et al. FGF regulates TGF-β signaling and endothelial-to-mesenchymal transition via control of let-7 miRNA expression. *Cell reports*. 2012;2(6):1684–1696.
19. Cooley BC, et al. TGF-β signaling mediates endothelial-to-mesenchymal transition (EndMT) during vein graft remodeling. *Sci Transl Med*. 2014;6(227):227ra34.
20. Maddaluno L, et al. EndMT contributes to the onset and progression of cerebral cavernous malformations. *Nature*. 2013;498(7455):492–496.
21. Zeisberg EM, Potenta S, Xie L, Zeisberg M, Kalluri R. Discovery of endothelial to mesenchymal transition as a source for carcinoma-associated fibroblasts. *Cancer Res*. 2007;67(21):10123–10128.
22. Gasperini P, et al. Kaposi sarcoma herpesvirus promotes endothelial-to-mesenchymal transition through Notch-dependent signaling. *Cancer Res*. 2012;72(5):1157–1169.
23. Charles N, et al. Perivascular nitric oxide activates notch signaling and promotes stem-like character in PDGF-induced glioma cells. *Cell Stem Cell*. 2010;6(2):141–152.
24. Fan Y, et al. Profilin-1 phosphorylation directs angiocrine expression and glioblastoma progression through HIF-1α accumulation. *Nat Cell Biol*. 2014;16(5):445–456.
25. Hardee ME, Zagzag D. Mechanisms of glioma-associated neovascularization. *Am J Pathol*. 2012;181(4):1126–1141.
26. Soda Y, et al. Transdifferentiation of glioblastoma cells into vascular endothelial cells. *Proc Natl Acad Sci USA*. 2011;108(11):4274–4280.
27. Osterreicher CH, et al. Fibroblast-specific protein 1 identifies an inflammatory subpopulation of macrophages in the liver. *Proc Natl Acad Sci USA*. 2011;108(1):308–313.
28. De Palma M, et al. Tie2 identifies a hematopoietic lineage of proangiogenic monocytes required for tumor vessel formation and a mesenchymal population of pericyte progenitors. *Cancer Cell*. 2005;8(3):211–226.
29. Takehara K, LeRoy EC, Grotendorst GR. TGF-beta inhibition of endothelial cell proliferation: alteration of EGF binding and EGF-induced growth-regulatory (competence) gene expression. *Cell*. 1987;49(3):415–422.
30. Lamouille S, Xu J, Derynck R. Molecular mechanisms of epithelial-mesenchymal transition. *Nat Rev Mol Cell Biol*. 2014;15(3):178–196.
31. Tomita N, et al. Angiogenic property of hepatocyte growth factor is dependent on upregulation of essential transcription factor for angiogenesis, ets-1. *Circulation*. 2003;107(10):1411–1417.
32. Wang H, Keiser JA. Hepatocyte growth factor enhances MMP activity in human endothelial cells. *Biochem Biophys Res Commun*. 2000;272(3):900–905.
33. Muller M, Morotti A, Ponzetto C. Activation of NF-κB is essential for hepatocyte growth factor-mediated proliferation and tubulogenesis. *Mol Cell Biol*. 2002;22(4):1060–1072.
34. Bussolino F, et al. Hepatocyte growth factor is a potent angiogenic factor which stimulates endothelial cell motility and growth. *J Cell Biol*. 1992;119(3):629–641.
35. Shojaei F, et al. HGF/c-Met acts as an alternative angiogenic pathway in sunitinib-resistant tumors. *Cancer Res*. 2010;70(24):10090–10100.
36. You WK, et al. VEGF and c-Met blockade amplify angiogenesis inhibition in pancreatic islet cancer. *Cancer Res*. 2011;71(14):4758–4768.
37. St Croix B, et al. Genes expressed in human tumor endothelium. *Science*. 2000;289(5482):1197–1202.
38. Streubel B, et al. Lymphoma-specific genetic aberrations in microvascular endothelial cells in B-cell lymphomas. *N Engl J Med*. 2004;351(3):250–259.
39. Seaman S, Stevens J, Yang MY, Logsdon D, Graff-Cherry C, St Croix B. Genes that distinguish physiological and pathological angiogenesis. *Cancer Cell*. 2007;11(6):539–554.
40. Ricci-Vitiani L, et al. Tumour vascularization via endothelial differentiation of glioblastoma stem-like cells. *Nature*. 2010;468(7325):824–828.
41. Wang R, et al. Glioblastoma stem-like cells give rise to tumour endothelium. *Nature*. 2010;468(7325):829–833.
42. Potenta S, Zeisberg E, Kalluri R. The role of endothelial-to-mesenchymal transition in cancer progression. *Br J Cancer*. 2008;99(9):1375–1379.
43. Kalluri R, Weinberg RA. The basics of epithelial-mesenchymal transition. *J Clin Invest*. 2009;119(6):1420–1428.
44. Thiery JP. Epithelial-mesenchymal transitions in tumour progression. *Nat Rev Cancer*. 2002;2(6):442–454.
45. Lu KV, et al. VEGF inhibits tumor cell invasion and mesenchymal transition through a MET/VEGFR2 complex. *Cancer Cell*. 2012;22(1):21–35.
46. Wang Y, et al. Ephrin-B2 controls VEGF-induced angiogenesis and lymphangiogenesis. *Nature*. 2010;465(7297):483–486.
47. Liu Y, et al. Somatic cell type specific gene transfer reveals a tumor-promoting function for p21(Waf1/Cip1). *EMBO J*. 2007;26(22):4683–4693.
48. Ciznadija D, Liu Y, Pyonteck SM, Holland EC, Koff A. Cyclin D1 and cdk4 mediate development of neurologically destructive oligodendroglioma. *Cancer Res*. 2011;71(19):6174–6183.